Breakthrough Technologies

Cellular Force Microscopy for in Vivo Measurements of Plant Tissue Mechanics[1][W][OA]

Anne-Lise Routier-Kierzkowska, Alain Weber, Petra Kochova, Dimitris Felekis, Bradley J. Nelson,
Cris Kuhlemeier, and Richard S. Smith*

Institute of Plant Sciences, University of Bern, CH–3013 Bern, Switzerland (A.-L.R.-K., A.W., P.K., C.K., R.S.S.);
Department of Mechanics, Faculty of Applied Sciences, University of West Bohemia, 306 14 Pilsen, Czech Republic
(P.K.); and Institute of Robotics and Intelligent Systems, Eidgenössische Technische Hochschule Zürich,
CH–8092 Zurich, Switzerland (D.F., B.J.N.)

Although growth and morphogenesis are controlled by genetics, physical shape change in plant tissue results from a balance between cell wall loosening and intracellular pressure. Despite recent work demonstrating a role for mechanical signals in morphogenesis, precise measurement of mechanical properties at the individual cell level remains a technical challenge. To address this challenge, we have developed cellular force microscopy (CFM), which combines the versatility of classical microindentation techniques with the high automation and resolution approaching that of atomic force microscopy. CFM's large range of forces provides the possibility to map the apparent stiffness of both plasmolyzed and turgid tissue as well as to perform micropuncture of cells using very high stresses. CFM experiments reveal that, within a tissue, local stiffness measurements can vary with the level of turgor pressure in an unexpected way. Altogether, our results highlight the importance of detailed physically based simulations for the interpretation of microindentation results. CFM's ability to be used both to assess and manipulate tissue mechanics makes it a method of choice to unravel the feedbacks between mechanics, genetics, and morphogenesis.

A major question in plant biology is how organs are able to develop complex three-dimensional (3D) shapes while maintaining mechanical integrity (Cosgrove, 2005; Thompson, 2005; Schopfer, 2006). Plant cells are surrounded by stiff cell walls that contain the considerable turgor pressure within (Schopfer, 2006). Although morphogenesis occurs at the tissue level (Coen et al., 2004), wall mechanical properties are controlled at the cellular level through the deposition and chemical modification of cell wall material (Köhler and Spatz, 2002; Baskin, 2005; Cosgrove, 2005; Burgert, 2006; Schopfer, 2006). Hence, the mechanical properties of the cell walls have to be studied in planta, at the cellular and subcellular scales (Geitmann, 2006; Mirabet et al., 2011).

The stiffness of a material is determined by the force that is required for a certain deformation. In single cells, stiffness can be investigated in situ using micro- and nano-indentation methods (Geitmann, 2006). A thin probe indents the cell surface, while both the applied load and the probe displacement are moni-

tored. Stiffness values are extracted by computing the slope of the force-displacement curve at maximal indentation depth. The stiffness obtained reflects not only cell wall elastic properties but also turgor pressure (Smith et al., 1998; Wang et al., 2004), cell and indenter geometry (Bolduc et al., 2006), and mechanical stresses prior to indentation (Zamir and Taber, 2004). For that reason, we will refer to it as "apparent stiffness" (Zamir and Taber, 2004). The influence of each factor on the apparent stiffness depends on the probe tip shape, its size, and how deep it is indented into the cell surface or how large the applied load is. For instance, it has been reported that the forces measured by using very large, spherical probes at a relatively small indentation depth are mainly due to the cell internal pressure (Lintilhac et al., 2000; Wei et al., 2001), because stretching of the cell wall is negligible. In pollen tubes, the apparent stiffness has been measured using microindentation methods with small, flat-tipped probes that were applying forces in the low micronewton range (Geitmann and Parre, 2004; Parre and Geitmann, 2005; Zerzour et al., 2009). Recently, nano-indentation with atomic force microscopy (AFM) has been used to study cells in the Arabidopsis (*Arabidopsis thaliana*) inflorescence apex (Milani et al., 2011; Peaucelle et al., 2011). Peaucelle and coworkers (2011) were able to detect differences in the cell apparent stiffness in relation to the degree of methylesterification of homogalacturonan, a pectic polymer. The measurements, however, were performed only on plasmolyzed tissues. In the study of Milani et al. (2011), very local differences in wall mechanical properties were detected by shallow indentation with a sharp, pyramidal indenter, using
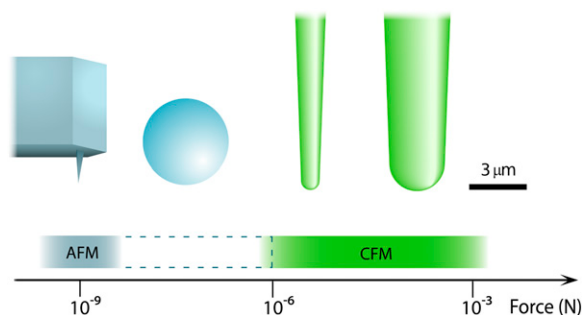
Figure 1. Comparison of tip sizes and forces used in nano-indentation and CFM studies on plants. AFM (in blue) was used by Milani et al. (2011) with a pyramidal indenter of 40 nm diameter and maximal forces of approximately 100 nN. Peaucelle et al. (2011) extended the working range of AFM in plant tissue (dotted blue line) by using stiffer cantilevers (up to 110 N m^{-1}) on which glass beads of 5 μm in diameter were glued manually. We used CFM (in green) for stiffness mapping with forces around 4 to 10 μN and hemispherical tip diameter of 2 to 3 μm. The use of rounded tips allows avoiding stress concentration inherent to sharp indenters. Puncture of the cell wall was obtained with a tip of 1 μm in diameter and forces up to 1 mN. Bar = 3 μm.

forces in the nanonewton range (Fig. 1). Hence, the cell wall was essentially compressed over a submicrometric volume, measuring the elastic modulus in the direction normal to its surface, as opposed to wall elasticity in the surface plane (Milani et al., 2011). Given the composite structure of the cell wall (Baskin, 2005; Cosgrove, 2005; Thompson, 2005; Schopfer, 2006), the wall elastic modulus is expected to be much lower in the transverse direction than parallel to the surface plane (Jäger et al., 2011; Milani et al., 2011). Since growth depends primarily on the in-plane deformation of the cell wall, it is thus important to measure directly in-plane elasticity.

Available microindentation devices are well suited to study in-plane mechanical properties of the cell wall, but they are limited by a lack of automation that precludes high-resolution scanning of surfaces. Nano-indentation using AFM offers a much higher level of resolution and automation; however, the forces and/or probe size usually used are too small to sufficiently stretch the cell wall on turgid tissues. We have developed a technology called cellular force microscopy (CFM) that combines the advantages of AFM with classical microindentation. CFM is an automated, high-resolution microindentation system capable of applying forces from the submicronewton to the milli-newton range (Fig. 1). The large range of forces allows the measurement of cell wall elastic properties and provides the possibility to indent very deeply into the cells, up to the point of cell wall rupture. High-resolution 3D maps of surface topography and apparent stiffness can be extracted with CFM, performing non-invasive raster scans on both turgid and plasmolyzed tissues. Automatic analysis of force-displacement curves is used to correct the measured stiffness for errors induced by the angle of indentation. CFM with high loads can be used for micropuncture experiments,

similar to micropenetration techniques (Hiller et al., 1996) and single cell compression (Blewett et al., 2000; Wang et al., 2006) to provide insight into the cell wall properties at very large deformation as well as local wall strength. Direct comparison between the turgid and nonturgid states of the cell without subjecting the cells to changes in medium is also possible, since micropuncture and force measurement can be done with the same probe.

RESULTS

Design and Operation of the CFM Device

The CFM apparatus is composed primarily of commercially available components: a single-axis capacitive force sensor (Sun and Nelson, 2007) mounted on a three-axis microrobotics actuator (Felekis et al., 2011). The setup is fixed on top of a standard inverted light microscope and isolated from external sources of vibration (Supplemental Fig. S1). Software developed in LabView is used to control the experimental procedure and acquire data (Felekis et al., 2011). A data-analysis software was developed that automatically extracts the indentation point and apparent stiffness values from the data. These are used to reconstruct the surface topography and produce stiffness maps.

The positioning technology of the microrobot is based on piezoelectric actuators. Two modes of actuation are available, a fast-stepping mode used over long distances (up to several centimeters) and a continuous mode for very precise, smooth oscillatory movements over short distances (up to 2 μm), with a resolution of 10 nm. The stepping mode is used while positioning the sensor prior to indentation, to find the sample surface during the initial approach, and for measurements where large movements are required. The continuous mode, being much more accurate than the stepping mode, is used during stiffness measurements (Supplemental Fig. S2). We used two types of capacitive force sensors with different flexure stiffness (approximately 180 and 800 newton [N] m^{-1}), which can measure force up to 160 and 2,000 μN, respectively. The hemispherical probe tip diameter is chosen depending on the usage; in the applications presented here, it varied between 1 μm for the puncture experiments and 2 to 3 μm for noninvasive measurements (Fig. 1). Combining the available tip sizes and the sensor force range, the probe can apply stresses comparable to the turgor pressure (a few bars) up to values 2 orders of magnitude higher. These forces produced indentations of a few micrometers to dozens of micrometers into the cells, either mildly stretching the cell wall or deforming it to the point of rupture.

Measurements are typically made by first moving the probe using the stepping mode, indenting the sample surface until reaching a user-specified target force (Supplemental Fig. S2). For stiffness mapping, multiple measurements are performed at predefined locations to obtain raster scans of the sample surface

on large areas (covering up to 150 μm in this study). The target force is chosen so that the indentation depth is at least equal to the indenter radius. Starting from this indentation depth, the continuous mode is used to produce a series of smooth oscillations, indenting and retracting the tip over several hundred nanometers. Stiffness values are extracted from force-displacement data acquired during the continuous mode. Measurements performed far beyond the contact point present the advantage of being less prone to artifacts related to tip-sample contact (Cappella and Dietler, 1999), such as adhesion or an irregular surface due, for example, to the geometry of individual cells within a tissue (Peaucelle et al., 2011).

While the sample is indented by the sensor, its springs deflect by an amount depending both on the measured force and the sensor stiffness. The data-analysis software enables the correction of raw position signal for sensor deflection, given the sensor stiffness value obtained by calibration (see "Materials and Methods"). While detecting the contact point, the force signal is corrected for undesired offset (e.g. caused by liquid surface tension in wet conditions). After both force and position signals are corrected, the apparent stiffness is extracted from the multiple oscillations (usually two to three) and averaged separately for loading and unloading phases. Multiple oscillations are used to evaluate data reliability: for purely elastic behavior, valid measurements should show force-indentation curves that do not drift in time and are similar in loading and unloading phases (Supplemental Fig. S2). The contact points extracted from data obtained with raster scans are used to reconstruct the sample surface in 3D. An analytical model was used to determine the effect of the angle of indentation on measured stiffness (Fig. 2), assuming frictionless contact (Supplemental Materials Methods S1). This analytical model was confirmed by finite element method (FEM) simulation (Supplemental Fig. S4) and used to correct stiffness values for surface slope (Fig. 2).

For puncture experiments, the sensor probe indents the cell surface until reaching a force of several hundred micronewtons. In this case, data are acquired in the stepping mode, as opposed to the continuous mode, since displacement over dozens of micrometers is required to break the cell wall. As in the case for other measurements, the force and displacement signals are corrected before further analysis.

CFM Measurements on Living Tissue and Single Cells

Onion (*Allium cepa*) epidermal peels were used as a model of a monolayered, homogeneous tissue. Two types of experiments were conducted on epidermal cells with CFM: stiffness mapping with noninvasive, small indentation scans covering several cells, and cell wall puncture using very high forces. The mechanical effects of turgor pressure were investigated by mapping cell apparent stiffness in various states of plasmolysis as well as by comparing stiffness before and after releasing turgor pressure by puncture. Stiffness measurements on BY2 tobacco (*Nicotiana tabacum*) culture cells in normal medium demonstrated that CFM is also suitable for single plant cells. FEM was used to simulate indentation experiments on realistic cell and tissue models. Such simulations are essential to interpret often nonintuitive experimental results, giving new insight into cell and tissue mechanics.

For stiffness mapping of onion epidermis, the maximal force parameter was chosen in such a way that the indentation depth (1–2 μm) on turgid cells was small, compared with the cell diameter (approximately 40 μm). FEM-based simulations showed that this indentation depth and tip diameter (2–3 μm) were small enough not to induce a significant increase in turgor pressure during the measurements (Supplemental Results S1). Small forces (4–10 μN) were used in order to avoid irreversible deformation of the cell wall and triggering physiological responses that might lead to significant changes in the tissue mechanical

Figure 2. Effect of slope on the apparent stiffness. A, Microscopic view of a turgid onion epidermis during the measurements. The shadow of the indenter is visible in the top part of the photograph. The black rectangle indicates the scanned area of the tissue. Bar = 40 μm. B, Color map of the angle (°) formed between the cell surface and the indenter probe. C, Color map of the apparent stiffness (N m^{-1}) measured during the scan. D, Color map of the corrected stiffness (N m^{-1}) computed using the measured stiffness, the surface slope, and the bending stiffness of the indenter probe.
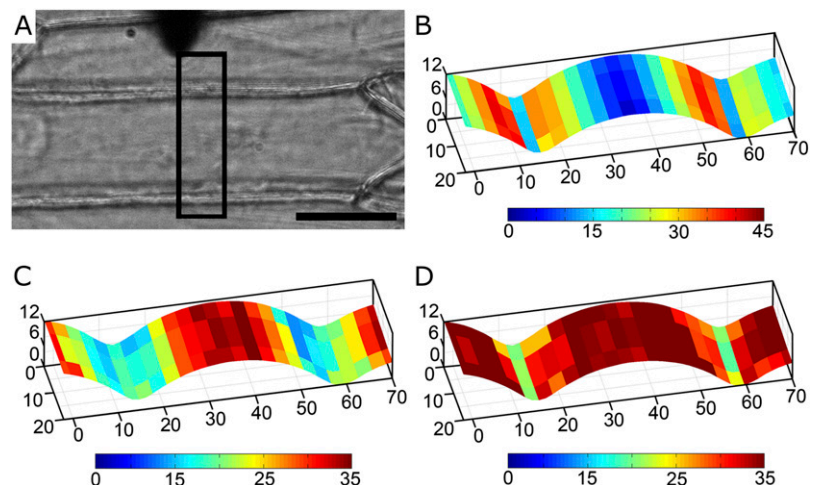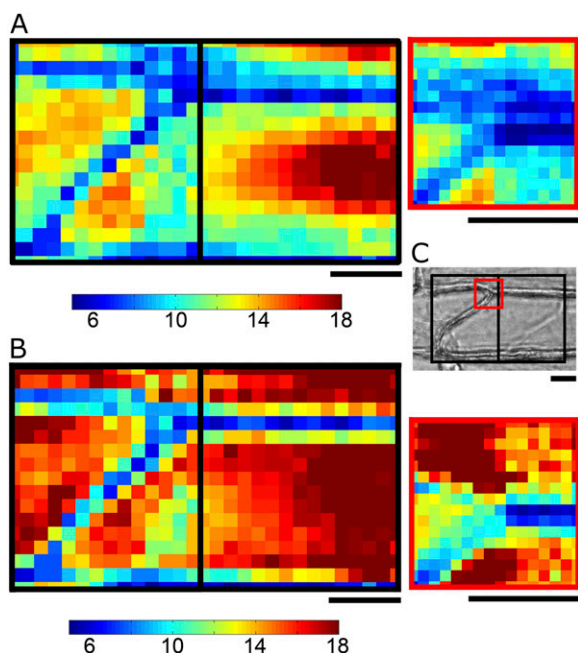
Figure 3. In a fully turgid epidermis, the apparent stiffness is lower over cross walls than on the top of the cells. A, Black rectangles show maps of measured stiffness over two areas of 64 × 52 μm. Note that the surface over the cross walls, in blue, is softer. The red square shows a finer scan of surface of 30 × 30 μm, covering three cross walls. B, The measured stiffness presented in A, after correction for the effect of the surface slope on stiffness. The color scales show stiffness in N m^{-1}. C, Microscopic view of the scanned tissue, with the shadow of the indenter tip. Black rectangles show the area scanned with a lateral step size of 4 μm. The red square shows the area scanned with a 2-μm step size. Bars = 20 μm.

properties during the time of the experiments (Supplemental Fig. S5). Measurements were corrected for slope, tip bending, and sensor deflection. In turgid tissues, the apparent stiffness is approximately uniform overall, except in a small area (3–5 μm) above the cross wall (Figs. 2 and 3), where stiffness is between 1.4 and 2.2 times lower (n = 8 cells).

In order to investigate the effect of pressure on stiffness measurements, we released the turgor of onion cells by plasmolyzing them in hypertonic medium and then let the cells recover by allowing water to diffuse slowly back through the cuticle and top wall. Full restoration of pressure took more than 12 h. Three different phases could be distinguished in the recovery. During the first phase (approximately 6 h after plasmolysis), the cytoplasm slowly swelled without completely filling the space between the cell walls (Fig. 4). During this period, the internal pressure was very low and was carried only by the plasma membrane, without inducing significant strain in the much stiffer cell walls. Accordingly, the top surface of the tissue was flat and the apparent stiffness remained low (2.8 ± 0.2 N m^{-1}; n = 27 measurement points), being about 15% to 20% stiffer above the anticlinal cell walls (Fig. 4). A second phase started when the cytoplasm filled the whole internal space, with further increases in

cytoplasm volume resulting in cell wall strain and considerable mechanical stress. The tissue surface then started to bulge out as the internal pressure increased, and the cell middle became stiffer (Fig. 4). The apparent stiffness above the anticlinal wall increased at the same time, remaining approximately 15% to 20% stiffer than the cell middle. The tissue reached a stationary state of full turgidity when the recovery was complete. At this stage, the cells were bulged out and the middle of the cells were 5.7 times stiffer than in the plasmolyzed state (16 ± 1 N m^{-1}; n = 7 measurement points). However, creases between cells were then considerably softer (2.1 times) than the rest of the surface (Fig. 4).

In order to interpret this unexpected change in the stiffness pattern as the turgor pressure increased, we simulated microindentation of onion cells with FEM. Using a simple model of a pressurized tissue with homogeneous cells walls, the surface above anticlinal walls was always stiffer upon indentation, independen-
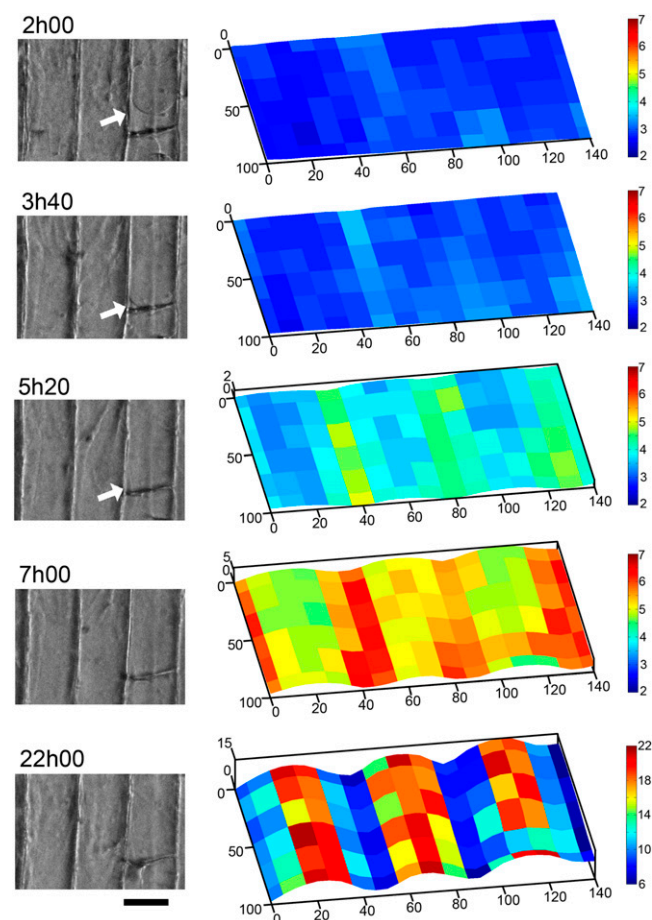

Figure 4. Changes in topography and measured stiffness in an onion peel recovering from plasmolysis. The left column shows microscopic views of the scanned area, covering three cells. Hours after plasmolysis are indicated. White arrows indicate cytoplasm filling the cell walls. The right column shows color maps of apparent stiffness (N m^{-1}) for the recovering peel. The color scale is the same (2–7 N m^{-1}) for the first four maps but different for the last stiffness map (6–22 N m^{-1}). Bar = 40 μm.
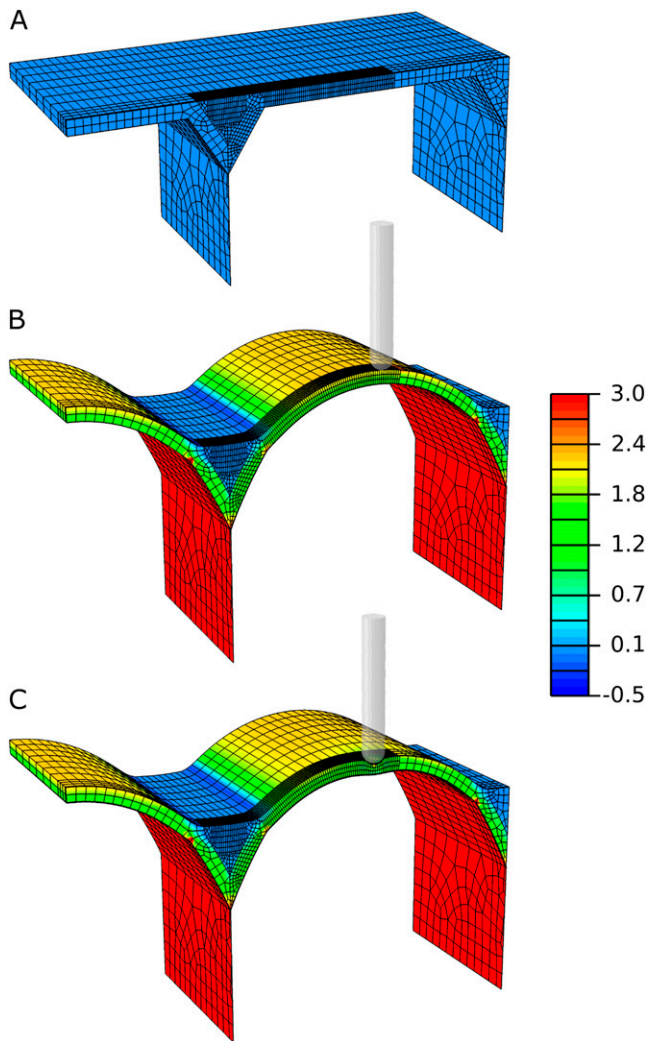
Figure 5. Sequential steps within a simulated indentation. Epidermal tissue is modeled by FEM using different elements for the anticlinal walls, top wall, and cuticle layer. A, Cut through the model length is shown in its initial state. B, The model is pressurized prior to indentation. C, Simulated indentation experiment. The color scale indicates maximum principal stress in MPa.

dently of the internal pressure. We could, however, reproduce the transition from stiffer to softer at the cell junctions by using a more realistic structural model based on cross-sections of onion epidermis (Suslov et al., 2009; Fig. 5). The junctions between the outer wall and the anticlinal walls were reinforced with a triangular gusset to match the shape of the cross-sections (Supplemental Fig. S8). In a plasmolyzed state, the apparent stiffness mainly reflects the bending stiffness of the upper cell wall (Supplemental Fig. S9). The presence of a gusset increases the bending stiffness locally, explaining why the tissue surface is stiffer at the cell junctions in the flaccid state (Supplemental Fig. S10). However, in order to fully reproduce the experimental results, the gusset material has to be much softer than the rest of the upper cell wall, which

is supported by the fact that it does not react with a cellulose stain (Suslov et al., 2009). As the cell surface bulges out due to the increasing turgor pressure, the thick upper cell wall surface becomes increasingly tense and stiff in the cell center. At the junctions, the tension due to cell internal pressure is borne by the cell wall layer underneath the soft gusset. Thus, the gusset itself is under slight compression, due to the cells bulging out on both sides (Fig. 5B). The apparent stiffness at cell junctions remains constant upon indentation, while the cell middle considerably stiffens with increased turgor pressure (Supplemental Fig. S10).

Besides stiffness mapping, CFM also enabled us to rupture the cell wall, resulting in the efflux of cell contents and the loss of turgor pressure (Supplemental Movie S1). Very high stresses had to be applied in order to rupture the wall in the middle of the cell (Fig. 6). During a single indentation, different events could be observed, which appeared as sudden changes in the force deformation curve (Fig. 6C). The first occurred at around 300 μN load and 10 μm indentation with a tip diameter of about 1 μm. During this first event, we observed a steep drop in load on a few hundreds nanometers. This appeared after a phase of constant
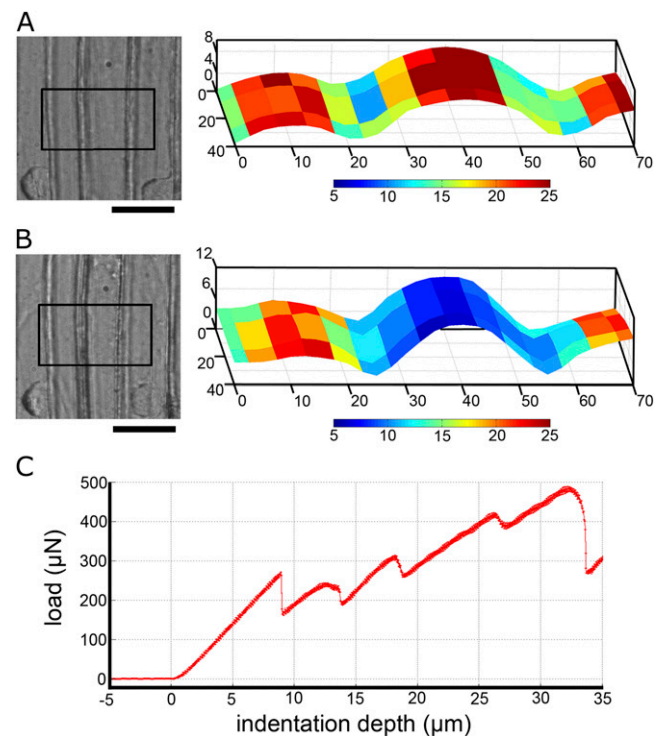
Figure 6. Puncture of the cell wall and effect of the release of turgor pressure on apparent stiffness. A, Light microscopy image and heat maps of the measured stiffness for the scanned region before puncture. B, Light microscopy image and stiffness map of the same region after puncturing the middle cell. The site of puncture is out of the image frame. Bars = 40 μm. C, Force-displacement signal during cell wall perforation. The first noticeable rupture occurs at around 9 μm indentation depth. The color scale indicates apparent stiffness in N m^{-1}.

load increase. After this first event, the slope of force versus the indentation curve was lower (Fig. 6). The subsequent number of drops in load varied, as well as the force and indentation for which they occurred. This could be due either to multiple layers in the cell wall structure (Cosgrove 2005) or to friction between the conical tip and the enlarging hole in the cell wall.

Using the same sensor as for the puncture, changes in surface geometry and apparent stiffness were monitored by stiffness mapping before and after the punctures. After rupturing the wall, a 4- to 5-fold decrease in the apparent stiffness was observed in the punctured cell, while the stiffness of adjacent cells remained roughly the same (Fig. 6, A and B). The curvature of the surface of the punctured cell increased after release of the turgor pressure by puncturing. Consistently, light microscopic observations revealed that the neighboring cells expanded into the area previously occupied by the punctured cell, which shrunk as the pressure was released (Fig. 6; Supplemental Movie S1). Before puncture, the apparent stiffness was highest on the cell top and lower on the cell flank, as usually observed in turgid cells. After puncture, the apparent stiffness on the top part of the cell was lower than on the flanks. Locally releasing turgor pressure by puncturing the top wall produced similar stiffness values as for plasmolyzed cells after correcting for geometry.

Experiments on BY-2 tobacco culture cells showed that CFM is also suitable for single cells. A major technical issue raised by these experiments was the adhesion of BY2 to the underlying flat surface, as the cells tend to slip under the indenter if the probe tip is not well positioned on the top of the cells. Thus, we did not perform raster scans on the cells but indented on a single point that we determined as being the cell center using light microscopy (Supplemental Fig. S3A). Measurements performed on four different subcultures in normal medium showed very consistent apparent stiffness. Overall, the median stiffness measured for BY2 cells was 6 ± 2 N m^{-1} ($n = 183$) with 3-μm-diameter indenter tip and a maximal force of 4 μN (Supplemental Fig. S3B). Note that for a similar probe tip diameter and higher force (10 μN), turgid onion epidermal cells were approximately five to six times stiffer (Fig. 2), showing that CFM can be used to measure samples of very different stiffness.

DISCUSSION

Flexibility of the CFM Setup

CFM is a new technology for fine measurements of mechanical properties over large areas of tissue. The long and thin sensor probes make it possible to measure regions that are difficult to access with other techniques. This setup also allows visualization of the indentation by a standard inverted light microscope. Stiffness measurements can be conducted both on very stiff, turgid tissue and on much softer culture cells.

Moreover, CFM offers the possibility to perform extremely precise micropuncture. This can be used for local measurement of cell wall strength (i.e. the force needed to break the wall). Cell-specific release of turgor pressure by puncture also modifies mechanical stresses locally, as in single-cell ablation experiments (Hamant et al., 2008), while avoiding damage due to laser heat. CFM can easily be assembled from commercially available components. Software for data acquisition and analysis are freely available upon request. Low cost, technical performance, and versatility make the CFM microrobotic system very attractive.

Data Interpretation and Modeling

Data interpretation is a major issue for any indentation measurements performed on nonhomogeneous samples. In order to decompose the apparent stiffness, an analytical or numerical model is needed. Previously, FEM simulations have been used to analyze the effects of geometrical factors on pollen tube apparent stiffness, such as cell size, wall thickness, and indenter tip radius, but did not take turgor pressure into account (Bolduc et al., 2006). Microcompression of single cells (Smith et al., 2000; Wang et al., 2004) was simulated with a pressurized thin-walled sphere squeezed between two plates (Smith et al., 1998); however, this kind of model is not suitable for microindentation experiments. To our knowledge, we built the first realistic FEM model to simulate microindentation on a tissue under turgor pressure. Our model shows that consideration of detailed tissue geometry and local differences in mechanical properties, as well as the level of turgidity, are essential for proper data interpretation. The model also highlights the importance of factors such as indentation depth (Supplemental Figs. S6 and S7), probe tip geometry, and the angle of indentation.

Influence of Turgor Pressure on the Measurements

Turgor pressure plays a very important role in microindentation experiments. Indeed, pressure induces tension in the walls that results in an increased apparent stiffness upon indentation (Zamir and Taber, 2004). This is analogous to the skin of a drum, which gets more difficult to press as one increases the tension while tuning the instrument. The stress itself may not be uniform, since it is strongly influenced by tissue geometry (Green, 1999; Dumais and Steele, 2000; Kutschera and Niklas, 2007; Hamant et al., 2008). By comparing stiffness maps for various levels of internal pressure, tip sizes, and indentation depths, cell wall local elastic properties can be untangled from the turgor-induced stress patterns. CFM could also be used to measure pressure directly and noninvasively, using the same principle as ball tonometry (Lintilhac et al., 2000; Wei et al., 2001). Cell wall elasticity could then be distinguished from turgor pressure for each cell on the organ surface.

Experiments using CFM provide new insights into tissue structure and mechanics. In a fully turgid tissue, the surface is softer above the cross walls than in the middle part of the cells (Fig. 3). This is in apparent contradiction to the cell junctions being stiffer under reduced turgor pressure (Fig. 4). Our FEM simulations suggest that this switch in stiffness pattern can be explained by tissue geometry and the presence of a much softer material accumulated between cells. CFM experimental results show that, in order to obtain a full picture of the sample's mechanical design, microindentations should be performed at various levels of turgidity and interpreted with a detailed mechanical model.

Potential Applications

In this study, we show that CFM can be used on live plant tissue and single cells under a wide range of forces and indentation depths. Previous work on mouse oocyte (Sun and Nelson, 2007) using the same type of sensors as in CFM indicated that their force range is suitable for animal systems as well. CFM scans can be performed over large areas, up to several centimeters wide, and on curved surfaces, opening the possibility to map organs such as Arabidopsis leaves or *Drosophila* wing discs. The axis of indentation can be horizontal as well as vertical, making it possible to measure living stems or roots in an upright position to avoid gravitropic responses. The CFM setup is small enough to be used in combination with confocal microscopy, enabling the visualization of fluorescent markers overlaid with stiffness maps for future studies. Monitoring of protein localization or cytoskeleton responses triggered by large deformations would also be possible. CFM versatility makes it the method of choice to unravel the feedbacks between mechanics, genetics, and growth.

MATERIALS AND METHODS

CFM Setup Description

The multiaxis positioning system is composed of three linear micropositioners (SmarAct SLC-2475) controlled by piezoelectric actuators. Each axis is capable of moving over a range of 49 mm and is calibrated by the manufacturer to give absolute position as an output. At the sampling frequency currently used for CFM, resolution of the positioning system is about 10 nm. A modular system (SmarAct MCS-3D) is used for control of the robot, both for manual positioning prior to experiments and automated control during experiments. The force sensor (Femtotools FT270 or FT540) is mounted on a custom aluminum arm (Femtotools), which is fixed to the microrobot (Supplemental Fig. S1). The positioning system is mounted on a custom-made stage on the top of an inverted microscope (Olympus IMT-2). The microscope is set on a vibration-free table and covered with a custom-made plexiglass box to protect the CFM components from environmental noise. The light source for microscopic observations is provided by light-emitting diodes on the top of the box, to avoid heating the setup, which would cause thermal expansion. The setup is also electrically grounded.

A data acquisition card (National Instruments USB 6009) is used to acquire force data from the sensor. The position of the robot is acquired through the modular control system (MCS-3D). Both components are connected to a personal computer via USB and integrated with a custom application implemented in LabView (National Instruments), which controls the positioning system based on a force feedback. The software user interface allows for controlling experiment parameters, such as contact force and maximal force (at deepest indentation), positioning speed, step size for raster scans, and number of loading cycles (Felekis et al., 2011).

Sensors Used in Experiments

Two types of uniaxial capacitive microforce sensors were used in the experiments: FT-S540, with a load range of ±160 μN and a resolution of 0.05 μN, and FT-S270, with a load range of $\pm2,000$ μN and resolution of 0.4 μN at 100 Hz (Femtotools; http://www.femtotools.com). In most experiments, FT-S540 was used, because of its higher resolution. FT-S270 was used when higher forces were required, such as when puncturing the upper cell wall of onion (*Allium cepa*) epidermis.

In all the experiments described, we used sensors on which a tungsten probe (Picoprobe; GGB Industries) was glued with a UV-curable glue. The probes are long cylinders, tapered at the extremity, ending with half-spheres of various radii. The total length of the probe is between 1 and 2 mm. The diameter of the cylindrical part is 22, 35, or 60 μm depending on the diameter of the ending half-sphere, 1, 2, or 3 μm, respectively. The smallest tip size, 1 μm in diameter, was used in combination with a FT-S270 sensor for puncture experiments. Intermediate and larger tip sizes were used with FT-S540 sensors for all other experiments on onion epidermis and tobacco (*Nicotiana tabacum*) BY2 cells.

Parameters Used for Experiments

Each measurement started with a fast-approach phase (average speed around 4 μm s^{-1}), using the stepping mode ("slip-stick" principle) of piezoelectric actuation. Once the sample surface was detected, the sensor moved backward by a user-defined amount (usually 1–3 μm). A second approach phase started with a lower speed (average speed of 1.5 μm s^{-1}), still using the stepping mode of actuation. During this "fine-approach" phase, the sensor indents the sample until reaching a user-defined target force. This triggers the last phase of measurement, where smooth oscillations are performed with the continuous mode of actuation (controlled directly by piezoelongation; Supplemental Fig. S2A). The average speed varied between 600 and 800 nm s^{-1} during the loading and unloading phases of the oscillations.

Depending on the type of experiment, the sample apparent stiffness, and the tip size, different values were used for the maximal force. For noninvasive scans on turgid onion peels (Figs. 2, 3, and 6) and on tissue recovering from plasmolysis (Fig. 4), maximal forces of 10 and 6 μN were used, respectively. For puncture of onion cell wall with FT-S270 sensors (Fig. 6), a maximal force of 600 μN was used. Experiments on BY2 cells were performed using a maximal force of 4 μN.

System Calibration

Before all experiments, the sensor stiffness was measured by acquiring force-displacement curves while indenting a hard surface (microscope glass slide or steel block). Assuming a negligible indentation depth compared with deflection of sensors springs, the measured stiffness was considered to closely approximate the bending stiffness of the beam springs themselves. A 5 $\times$ 5 grid was performed, with a maximal force of 40 μN and the same velocity parameters as those used in subsequent experiments. The grid was repeated until the extracted stiffness varied less than 5% in all the grid nodes. Typical stiffness values varied for individual FT-S540 sensors between 150 and 200 N m^{-1}. For FT-S270, it varied between 600 and 800 N m^{-1}. Before each experimental session, the sensors were checked for drift and/or damage by comparing stiffness values with those taken upon their first use.

Data Analysis

The code used for data analysis was written in Matlab (Mathworks).

Correction for Sensor Deflection

During measurements on soft samples, the sensor probe indents the sample surface while the sensor's beam springs bend by an amount depending on the applied load. Thus, for a given position z of the actuator, the actual probe tip $z_{corrected}$ position relative to the sample is as follows:

$$z_{corrected} = z + F/S$$

where F is the load measured by the sensor and S is the sensor stiffness determined by calibration. The sign convention for z and F vectors is the same (positive is pointing upward).

Detection of the Contact Point (Sample Surface) and Force Offset

The contact point between the sensor probe and the sample surface is extracted from the force-displacement curve acquired during the fine approach. In the ideal case, the force measured by the sensor during the fine approach is zero before contact. The force signal will increase rapidly as the probe tip contacts the sample and indents farther into the material. The contact point should then be the first point in the force-displacement curve that has a positive value. Due to various factors (water surface tension, vibrations during stepping mode, etc.), the force signal is often noisy and nonzero before contact. Thus, in order to find the contact point, we first smooth both the displacement and force signals using a Savitzky-Golay filter (Supplemental Fig. S2C). For each measurement cycle, the force signal is offset, so that the mean force signal before the contact point is equal to zero. The contact point is then determined to be the closest point to the maximal indentation that is below a user-defined contact force threshold (usually smaller than 1 μN). Both force offsetting and contact point detection are performed iteratively, using finer and finer threshold values. Indentation depth is then given by the sensor position (corrected for sensor deflection) minus the contact point position. We call the maximal indentation depth the value corresponding to the last point reached during the fine approach phase. The force signal offset is used further to deduce the actual load exerted on the sample at maximal indentation depth.

Computation of Stiffness

The stepping mode of actuation during the fine approach results in data that are more noisy than for the continuous mode (Supplemental Fig. S2, A and B). Therefore, stiffness values are extracted from force-displacement curves acquired during the smooth oscillations in continuous mode. We compute the stiffness as the slope of a least-squares linear fit of the force-displacement curve, close to maximal indentation depth. Points used for the linear fit are the ones above a user-defined force threshold, thus avoiding points that are too close to the contact point. The linear fit threshold, usually equal to half of the maximal force, is chosen so that the points taken for the linear fit are typically not farther than 400 nm from the point of maximal indentation depth (Supplemental Fig. S2D). Curves corresponding to loading and unloading phases are analyzed separately. Stiffness values given in this article correspond to the loading phase, since they are less influenced by adhesion between the tip and the sample (Cappella and Dietler, 1999).

3D Reconstruction and Visualization of Sample Surface

For each (x, y) position of the raster scan grid, we extract a contact point (giving the z position) as well as other parameters (stiffness, maximal indentation depth, maximal force, creep). For each point, the normal to the surface is computed, using a bicubic fit of the point and its closest neighbors. Surface slope is then given by the angle formed by the normal to the surface and the z axis. In order to visualize parameter values on 3D curved surfaces, a rectangular grid is created, such that the center of each rectangle corresponds to the (x, y, z) position of a measurement point. The z position of the rectangle corners are then obtained by a cubic interpolation. Coloring of each rectangle corresponds directly to the parameter value (e.g. stiffness) extracted for the corresponding measurement point.

Effect of Indentation Angle on Measured Stiffness

Indenting on a surface that is not perpendicular to the sensor probe modifies the measured stiffness. We studied this effect, assuming that the contact between the spherical tip and the sample was frictionless and the tip probe could bend under the applied load (Supplemental Materials and Methods S1). For an angle of indentation a and given the probe-bending stiffness S_B, the measured stiffness S_z is related to the "normal" stiffness S_n (the stiffness that would be measured with a probe normal to the surface) by

$$S_z = S_n \cdot S_B \cdot cos(a)^2 / (S_B + S_n \cdot sin(a)^2)$$

and

$$S_n = S_z \cdot S_B / (S_B \cdot cos(a)^2 - S_z \cdot sin(a)^2)$$

Using the last equation, we computed the stiffness normal to the surface from the measured stiffness, the surface slope obtained from raster scan data,

and the probe-bending stiffness. The analytical model was confirmed by FEM simulations (Supplemental Results S1).

Comparison of Stiffness Measured on the Top and Junctions in Onion Epidermal Cells

Stiffness values for the cell top and junctions were extracted from stiffness maps. Measurement points were classified as belonging to the junctions if their z position was low and the slope was below 20° and as belonging to the top if the z position was high and the slope was below 20°. We then computed the ratio between the median of stiffness values for points belonging to the top and junctions. For the statistics on turgid epidermis, we extracted data from stiffness maps that covered eight different regions on a total of six independent peels.

FEM Simulations of Microindentation of Tissue under Partial and Full Turgor Pressure

To explain the stiffness maps obtained during the recovery of turgor pressure in epidermal cells (Fig. 4), we modeled the CFM experiment with different turgor pressures. The model was built in Abaqus Standard (SIMULIA). We did not try to quantify model parameters but to capture the qualitative behavior of the experiment. The geometry and constitutive parts of the model were based on histological sections reported previously (Suslov et al., 2009). The top cell wall layer was assumed to be composed of a thin, stiff layer covered by a much thicker and softer layer, presumably the cuticle. Above the cross walls in the crevice, the top layer is assumed to consist of even softer material, based on the observation that these places did not react to cellulose staining (Suslov et al., 2009). The bottom part of the model is given by two parallel cross walls, each 15 μm high, which are 40 μm apart from each other. The middle cross wall is twice as thick (1 μm) as the distal one, because it represents the cell walls of two neighboring cells. Both cross walls are tied to a solid region that covers the upper part of the model. This region is composed of a solid cutical layer of 2 μm thickness that is reinforced by a membrane skin (0.5 μm) at the bottom surface. The region above the cross wall and the cutical layer is filled up with a prismatic gusset (7.66 μm wide, 6.18 μm high). The CFM indenter is modeled by a rigid hemisphere (3 μm diameter) that is attached to a rigid cylinder. All sections were assigned with linear elastic, isotropic material definitions (Supplemental Fig. S8A). The resulting geometry was further partitioned into two regions of different mesh properties. Those areas that would be involved in the contact problem were meshed with linear membrane (M3D4) and linear solid (C3D8, C3D6) elements. The remaining structure was meshed with quadratic membrane (M3D6, M3D8) and quadratic solid (C3D20, C3D15) elements. The domains of different element degrees as well as the two edges between cross walls and the upper cell wall were connected by tie constraints. The simulation was divided into an inflation step and an indentation step that were both performed under the same boundary conditions (Fig. 5). During the inflation step, the structure was pressurized with either 5 bar (turgid) or 0.1 bar (deflated). For both pressures, we then simulated indentations at different positions. The contact was assumed to be frictionless and enforced by a finite sliding, node-to-node contact algorithm. To handle large distortions of the mesh, we used Arbitrary Langrangian Eulerian remeshing around the zone of contact.

Sample Preparation

Fresh spring onions were acquired commercially. For all experiments, we used the white, lower part from the second scale of the bulb. The excision was made a few millimeters from the bulb base and around 2 cm long for 1 cm wide. Waterproof laboratory tags were stuck to the extremities of the bulb piece on its adaxial side and then gently lifted so that the epidermis detached from inner bulb tissue. Next, epidermis peels were bathed in distilled water, hanging from the tagged extremities, for 10 min. For the plasmolysis experiments, the peels were additionally bathed for 2 min in 3% NaCl solution, then quickly rinsed with pure water in order to remove the remains of salt on the peel surface.

The bottom side of the peels (previously facing the inner tissue) was then gently dried using cellulose paper (Whatman). Using the tags at their extremities, peels were stuck to tissue culture frost-treated plastic plates for better adhesion of the cells to the dish. Two additional tags were stuck on the remaining free sides of the peels, so that the peels were held flat against the

dish. The prepared peels were then covered in distilled water before measurements. Since the tags are waterproof, water had to enter the cells by passing through the cuticle that covers the upper face of the epidermal peel. The cuticle is a thick hydrophobic layer whose physiological function, among others, is to prevent the cells from drying. The water diffused hence very slowly, resulting in a slow recovery of turgor pressure for the plasmolyzed peels.

Fresh cultures of BY2 tobacco cells were prepared between 1 and 3 d before CFM measurements. Experiments were performed in the same medium as used for cell culture in frost-treated tissue culture dishes. The cells were allowed to settle at the bottom of the culture dishes before starting measurements. Long, cylindrical cells (80–160 μm in length and around 45 μm in diameter) in files were chosen for the experiments (Supplemental Fig. S3). In order to make sure that the cells were properly adhering to the plate, we measured only cells that did not float in the medium while moving the plate.

Supplemental Data

The following materials are available in the online version of this article.

Supplemental Figure S1. CFM setup on inverted microscope.

Supplemental Figure S2. Computation of contact point and stiffness from force and position data.

Supplemental Figure S3. CFM measurements on BY-2 culture cells.

Supplemental Figure S4. FEM verification of an analytical model to correct for indentation angle.

Supplemental Figure S5. Results of repetitive scans on a turgid onion epidermis peel.

Supplemental Figure S6. Design of simulations used to determine the increase in pressure during indentation.

Supplemental Figure S7. Effect of indentation on internal pressure increase and measured stiffness.

Supplemental Figure S8. Structure of the FEM model of epidermal cells.

Supplemental Figure S9. Stress resulting from simulated indentation on cells with low and high pressure.

Supplemental Figure S10. Force indentation curves obtained from simulating indentations on cells with low or high pressure.

Supplemental Materials and Methods S1.

Supplemental Results S1.

Supplemental Movie S1. Micropuncture of onion epidermal cell.

ACKNOWLEDGMENTS

LITERATURE CITED

Baskin TI (2005) Anisotropic expansion of the plant cell wall. Annu Rev Cell Dev Biol **21:** 203–222

Blewett J, Burrows K, Thomas CA (2000) Micromanipulation method to measure the mechanical properties of single tomato suspension cells. Biotechnol Lett **22:** 1877–1883

Bolduc JE, Lewis LJ, Aubin CE, Geitmann A (2006) Finite-element analysis of geometrical factors in micro-indentation of pollen tubes. Biomech Model Mechanobiol **5:** 227–236

Burgert I (2006) Exploring the micromechanical design of plant cell walls. Am J Bot **93:** 1391–1401

Cappella B, Dietler G (1999) Force-distance curves by atomic force microscopy. Surf Sci Rep **34:** 5–104

Coen E, Rolland-Lagan AG, Matthews M, Bangham JA, Prusinkiewicz P (2004) The genetics of geometry. Proc Natl Acad Sci USA **101:** 4728–4735

Cosgrove DJ (2005) Growth of the plant cell wall. Nat Rev Mol Cell Biol **6:** 850–861

Dumais J, Steele CR (2000) New evidence for the role of mechanical forces in the shoot apical meristem. J Plant Growth Regul **19:** 7–18

Felekis D, Muntwyler S, Vogler H, Beyeler F, Grossniklaus U, Nelson BJ (2011) Quantifying growth mechanics of living, growing plant cells in situ using microrobotics. Micro Nano Lett **6:** 311–316

Geitmann A (2006) Experimental approaches used to quantify physical parameters at cellular and subcellular levels. Am J Bot **93:** 1380–1390

Geitmann A, Parre E (2004) The local cytomechanical properties of growing pollen tubes correspond to the axial distribution of structural cellular elements. Sex Plant Reprod **17:** 9–16

Green PB (1999) Expression of pattern in plants: combining molecular and calculus-based biophysical paradigms. Am J Bot **86:** 1059–1076

Hamant O, Heisler MG, Jönsson H, Krupinski P, Uyttewaal M, Bokov P, Corson F, Sahlin P, Boudaoud A, Meyerowitz EM, et al (2008) Developmental patterning by mechanical signals in Arabidopsis. Science **322:** 1650–1655

Hiller R, Bruce D, Jeronimidis G (1996) A micro-penetration technique for mechanical testing of plant cell walls. J Texture Stud **27:** 559–587

Jäger A, Hofstetter K, Buksnowitz C, Gindl-Altmutter W, Konnerth J (2011) Identification of stiffness tensor components of wood cell walls by means of nanoindentation. Compos Part A: Appl Sci **42:** 2101–2109

Köhler L, Spatz HC (2002) Micromechanics of plant tissues beyond the linear-elastic range. Planta **215:** 33–40

Kutschera U, Niklas KJ (2007) The epidermal-growth-control theory of stem elongation: an old and a new perspective. J Plant Physiol **164:** 1395–1409

Lintilhac PM, Wei C, Tanguay JJ, Outwater JO (2000) Ball tonometry: a rapid, nondestructive method for measuring cell turgor pressure in thin-walled plant cells. J Plant Growth Regul **19:** 90–97

Milani P, Gholamirad M, Traas J, Arnéodo A, Boudaoud A, Argoul F, Hamant O (2011) In vivo analysis of local wall stiffness at the shoot apical meristem in Arabidopsis using atomic force microscopy. Plant J **67:** 1116–1123

Mirabet V, Das P, Boudaoud A, Hamant O (2011) The role of mechanical forces in plant morphogenesis. Annu Rev Plant Biol **62:** 365–385

Parre E, Geitmann A (2005) Pectin and the role of the physical properties of the cell wall in pollen tube growth of Solanum chacoense. Planta **220:** 582–592

Peaucelle A, Braybrook SA, Le Guillou L, Bron E, Kuhlemeier C, Höfte H (2011) Pectin-induced changes in cell wall mechanics underlie organ initiation in Arabidopsis. Curr Biol **21:** 1720–1726

Schopfer P (2006) Biomechanics of plant growth. Am J Bot **93:** 1415–1425

Smith A, Moxham K, Middelberg A (1998) On uniquely determining cell-wall material properties with the compression experiment. Chem Eng Sci **53:** 3913–3922

Smith AE, Zhang Z, Thomas CR, Moxham KE, Middelberg AP (2000) The mechanical properties of Saccharomyces cerevisiae. Proc Natl Acad Sci USA **97:** 9871–9874

Sun Y, Nelson BJ (2007) MEMS capacitive force sensors for cellular and flight biomechanics. Biomed Mater **2:** S16–S22

Suslov D, Verbelen JP, Vissenberg K (2009) Onion epidermis as a new model to study the control of growth anisotropy in higher plants. J Exp Bot **60:** 4175–4187

Thompson DS (2005) How do cell walls regulate plant growth? J Exp Bot **56:** 2275–2285

Wang CX, Wang L, Thomas CR (2004) Modelling the mechanical properties of single suspension-cultured tomato cells. Ann Bot (Lond) **93:** 443–453

Wang L, Hukin D, Pritchard J, Thomas C (2006) Comparison of plant cell turgor pressure measurement by pressure probe and micromanipulation. Biotechnol Lett **28:** 1147–1150

Wei C, Lintilhac PM, Tanguay JJ (2001) An insight into cell elasticity and load-bearing ability: measurement and theory. Plant Physiol **126:** 1129–1138

Zamir EA, Taber LA (2004) On the effects of residual stress in micro-indentation tests of soft tissue structures. J Biomech Eng **126:** 276–283

Zerzour R, Kroeger J, Geitmann A (2009) Polar growth in pollen tubes is associated with spatially confined dynamic changes in cell mechanical properties. Dev Biol **334:** 437–446